MATHEMATICAL BIOSCIENCES
AND ENGINEERING
Volume **13**, Number **2**, April **2016**

doi:10.3934/mbe.2015011

pp. **443–460**

A MULTISCALE MODEL FOR GLIOMA SPREAD INCLUDING CELL-TISSUE INTERACTIONS AND PROLIFERATION

Christian Engwer and Markus Knappitsch

WWU Münster, Institute for Computational und Applied Mathematics
and Cluster of Excellence EXC 1003, Cells in Motion
Orleans-Ring 10
48149 Münster, Germany

Christina Surulescu*

TU Kaiserslautern, Felix Klein Center of Mathematics
Paul-Ehrlich-Str. 31
67663 Kaiserslautern, Germany

(Communicated by Yang Kuang)

Dedicated to Messoud Efendiev (Helmholtz Center Munich) on his 60th birthday.

Abstract. Glioma is a broad class of brain and spinal cord tumors arising from glia cells, which are the main brain cells that can develop into neoplasms. They are highly invasive and lead to irregular tumor margins which are not precisely identifiable by medical imaging, thus rendering a precise enough resection very difficult. The understanding of glioma spread patterns is hence essential for both radiological therapy as well as surgical treatment. In this paper we propose a multiscale model for glioma growth including interactions of the cells with the underlying tissue network, along with proliferative effects. Our current accounting for two subpopulations of cells to accomodate proliferation according to the go-or-grow dichtomoty is an extension of the setting in [16]. As in that paper, we assume that cancer cells use neuronal fiber tracts as invasive pathways. Hence, the individual structure of brain tissue seems to be decisive for the tumor spread. Diffusion tensor imaging (DTI) is able to provide such information, thus opening the way for patient specific modeling of glioma invasion. Starting from a multiscale model involving subcellular (microscopic) and individual (mesoscale) cell dynamics, we perform a parabolic scaling to obtain an approximating reaction-diffusion-transport equation on the macroscale of the tumor cell population. Numerical simulations based on DTI data are carried out in order to assess the performance of our modeling approach.

1. **Introduction.** Gliomas are malignant primary tumors in the human brain with a poor prognosis [50]. The common treatment approach involves surgical resection, usually followed by radiotherapy. Thereby, the assessment of the tumor margin is, however, a challenging issue, due to the high invasiveness of gliomas and their finger-like, often disconnected, fibrillary patterns [10, 12, 20, 35]. Mathematical

2010 *Mathematics Subject Classification.* Primary: 92C17, 92C50; Secondary: 35Q92.

Key words and phrases. Multiscale model, glioma invasion, kinetic transport equations, diffusion tensor imaging, macrosccopic scaling, reaction-diffusion-transport equations.

* Corresponding author.

models aim at providing enhanced information about position, shape, and extent of the tumor by relying on medical imaging techniques. In particular, diffusion tensor imaging (DTI) is one of the most common radiological methods in the detection of brain tumors [43]. On T1- and T2-weighted images neoplastic and healthy tissue differ in intensity, thus making the core part of the tumor visible.

DTI techniques are non-invasive and they permit to assess the specific brain architecture. Modern imaging methods rely on evaluating the diffusion behaviour of water molecules within structured tissue. This reveals the orientation and anisotropy (meaning the extent of joint alignment) of neuronal fibers making up white matter tracts. This information is particularly interesting for surgery and radiation therapy.

Several key features have been identified to be crucial for tumor progression, see e.g., [24]. In this work we focus on the interaction of tumor cells with the underlying tissue and on proliferative effects. The model we propose here has a multiscale character, with the purpose of connecting the various levels on which the relevant biochemical processes triggering glioma spread take place. For modeling tumor growth we rely on the *go-or-grow* hypothesis, which states that cancer cells can either move or proliferate [21, 29]. We assume that cancer cells use neuronal fiber tracts as invasive pathways, which makes the individual brain structure interesting for patient specific modelling of glioma. Diffusion tensor imaging data are able to provide this information [45, 46].

Starting in Section 2 with a kinetic model on the mesoscale and an ODE on the subcellular level, a parabolic scaling yields an approximating reaction-diffusion-transport equation on the macroscale. Thereby, the precise form of the coefficients is determined in direct relationship with the available DTI data. Section 3 is concerned with the numerical simulation for the macroscopic equation. Eventually, in Section 4 we comment on the performance of this modeling approach.

1.1. **Multiscale modelling of glioma growth.** The invasion of tumor cells is a highly complex process involving a plethora of phenomena on different spatial and temporal scales [24]. Multiscale models can help to map this high degree of complexity into mathematical structures. Such mathematical settings involve two or several scales and accordingly more or less details of the processes they describe. Micro-macro models for tumor cell migration have been proposed and analysed e.g., in [37], which accounts for the effect of heat shock proteins (microlevel) on cancer invasion (on the macrolevel) and extends the model in [44], or more recently for the migration of cancer cells performing haptotaxis and chemotaxis (macroscale) under the influence of integrin binding to soluble and unsoluble ligands (microscale) [36, 42] or for the acid-mediated tumor invasion with pH taxis [41]. Different, but related approaches are hybrids between discrete and continuous modeling. These use cellular Potts or (lattice gas) cellular automata to provide lattice based simulations of individual cells involving more or less details on the subcellular level, from which information about the behavior on the population level can be extracted, see e.g., [9, 25] and the references therein. More complex continuum models also involving mesoscale dynamics (individual cell-tissue and/or cell-cell interactions) were considered by Bellomo et al. [5, 6, 7] or – fitting in the same framework – in e.g., [16, 30, 31, 34, 39].

In our model for glioma growth and spread we distinguish between three different scales. The *microscale* refers to processes happening on the subcellular level. In our setting these reduce to the binding of cell surface receptors to unsoluble ligands

and we employ an ordinary differential equation for the corresponding mass action kinetics. The *mesoscale* accounts for the behavior of individual cells and their interactions with their surroundings, in this case the (anisotropic) tissue network. The dynamics are characterized with the aid of kinetic transport equations for the densities of moving and resting cells (see Section 2.3). At this point, we rely on the above mentioned *go or grow* dichotomy. Finally, the *macroscale* refers to the population level on which the tumor as a whole can be observed. Unlike the previous two scales, it is not included in the original model, but deduced from it. More precisely, it is our goal in this paper do derive an equation for the macroscopic density $N(t, \mathbf{x})$ of tumor cells at time t at position $\mathbf{x}$, which also contains the information of the descriptions of the micro- and mesoscales.

1.2. **Diffusion tensor imaging.** At present, medical imaging methods like *computed tomography* (CT) along with magnetic resonance imaging based methods like *diffusion tensor imaging* (DTI) play a central role in the diagnosis of brain tumors in general. Cancerous tissue and healthy tissue differ in intensity in the representation, and hence malignant tissue alterations can be observed. One significant shortcoming is that not the whole tumor is visible, but only its core part. The actual tumor margin cannot be assessed. This is a major drawback, since after resection of the malignant region visible on DTI or CT scans the tumor can start growing again due to the incomplete removal.

However, in particular the diffusion tensor imaging (DTI) method is of high value for glioma prognosis as it provides information about the local tissue structure within the brain [46]. DTI relies on the measurement of the diffusion behaviour of water molecules within structured tissue, relating it to the anisotopy of neural fiber tracts [15, 45]. The water molecules are assumed to diffuse faster along fiber structures than orthogonally to them, which allows to capture the mentioned anisotropy. Technically, DTI measures the apparent diffusivity of water molecules per volume element (voxel). This can be characterized with the (symmetric) *water diffusion tensor*

$$\mathbb{D}_W(\mathbf{x}) = \begin{pmatrix} d_{xx}(\mathbf{x}) & d_{xy}(\mathbf{x}) & d_{xz}(\mathbf{x}) \\ d_{yx}(\mathbf{x}) & d_{yy}(\mathbf{x}) & d_{yz}(\mathbf{x}) \\ d_{zx}(\mathbf{x}) & d_{zy}(\mathbf{x}) & d_{zz}(\mathbf{x}) \end{pmatrix}.$$

Thereby, the diffusion tensor can be visualized e.g., with the aid of the *fractional anisotropy index* [8] or with *tensor glyphs*. While the former is a scalar value between zero and one, computed by using the eigenvalues of the apparent diffusion tensor[1], the latter convey tensor variables by mapping the tensor eigenvectors and eigenvalues to the orientation and shape of e.g., a cuboid or an ellipsoid. Glyphs commonly used in this context are *ellipsoids* and *peanuts*. For more details on this topic we refer to [16] and the references therein.

Tractography aims to reconstruct the local tissue orientation out of DTI data [14]. This is a quite complex process and still part of ongoing research. As we are primarily interested in one main direction of tissue fibers per voxel, we will use a simple mathematical expression to connect the water diffusion tensor and the local fiber distribution in Section 2.4.

[1]A value close to one means high anisotropy, i.e., a strong preference for a specific direction, whereas a very small value corresponds to the nearly isotropic case.

2. A multiscale model including proliferation.

2.1. Transport equations with resting phases.

We aim at providing a multiscale model for glioma spread wich includes proliferation and interactions of the cells with the extracellular matrix. It has been proposed that the go-or-grow hypothesis is a good starting point in modeling proliferative effects on the cell scale [9, 25]. Here we start from the approach in [26] and propose a setting which is expanded by a model for the cell receptor dynamics on the microscale as in [16] and which also accounts for the interaction between tumor cells and tissue fibers.

We observe the density functions $p(t, \mathbf{x}, \mathbf{v}, \mathbf{y})$ of moving cells at time t, position $\mathbf{x} \in \mathbb{R}^n$, velocity[2] $\mathbf{v} \in V \subset \mathbb{R}^n$, and internal state $\mathbf{y} \in Y \subset \mathbb{R}^d$ and of resting (and hence proliferating) cells $r(t, \mathbf{x}, \mathbf{y})$. This leads to a system of equations of the form

$$\partial_t p + \nabla_{\mathbf{x}} \cdot (\mathbf{v}p) + \nabla_{\mathbf{y}} \cdot (\mathbf{G}(\mathbf{y})p) = \mathcal{L}[\lambda]p - \alpha(\mathbf{x})p + \frac{\beta q}{\omega} r - l(N)p, \tag{1a}$$

$$\partial_t r = \alpha(\mathbf{x}) \int_V p d\mathbf{v} - \beta r + g(N)r - l(N)r. \tag{1b}$$

Here

$$\mathcal{L}[\lambda]p := -\lambda(\mathbf{y})p + \lambda(\mathbf{y}) \int_V K(\mathbf{x}, \mathbf{v}) p(\mathbf{v}') d\mathbf{v}' \tag{2}$$

is the *turning operator* modeling the cell velocity innovations due to contact guidance, environmental cues etc. These influences are contained in the turning kernel K. As proposed in [27] and used in [16], we choose $K(\mathbf{x}, \mathbf{v}) = \frac{q(\mathbf{x}, \hat{\mathbf{v}})}{\omega}$, where $\hat{\mathbf{v}}$ is the normalized velocity, $q(\mathbf{x}, \hat{\mathbf{v}})$ is the directional distribution of tissue fibers, and $\omega = \int_V q(\hat{\mathbf{v}}) d\mathbf{v} = s^{n-1}$ is a scaling constant. The function $\lambda(\mathbf{y})$ denotes the *turning rate* of cells. The vector $\mathbf{y}$ stands for the internal state of a cell: its components can be, for instance, concentrations of proteins involved in some intracellular signaling network or – as will be the case throughout this work – the concentration of cell surface receptors bound to tissue elements in their environment.[3]

As integrins expressed by resting cells cannot in general bind their ligands (see e.g., [38]), we assume this also for the cell surface receptors acting in our model. This allows us to omit the corresponding supplementary term for the 'transport' w.r.t. y present in (1a).[4]

The receptor binding dynamics is characterized by an ordinary differential equation

$$\frac{d}{dt} y(t) = G(y(t), A),$$

where the right hand side is involving the volume fraction of tissue $A(t, \mathbf{x})$ (including ECM and brain fibers) as input, see [16]. For simplicity we account in this work only

[2] We assume for simplicity $V = s\mathbb{S}^{n-1}$, with s some positive constant, hence we are only interested in the direction of the velocity and not in its speed; thereby, $\mathbb{S}^{n-1}$ denotes the unit sphere in $\mathbb{R}^n$.

[3] Integrins (cell surface transmembrane heterodimers) binding to ECM play an essential role in glioma invasion [13, 47]. On the other hand, it is largely accepted that glioma follow white matter tracts [11, 21, 22], but little is known about the way they interact with these. As integrins do not seem to directly bind to the myelinated axons, there might be some further receptors responsible for such binding or the interaction is rather indirect; adapting the description in [47] one can imagine the glioma cells 'climbing' along a ladder whose long 'rails' are myelinated axons and whose 'rungs' are made up of the ECM fibers present in the space between myelinated axons, oligodendrocytes, astrocytes etc.

[4] Including this term is, however, no challenge, as this situation can be handled in the same way.

for binding of cell surface receptors to unsoluble components of the tissue, modeled by A. This assumption reduces the above ODE system to just one equation for the receptor binding dynamics, see (3) below.

The function N in equations (1a) and (1b) denotes the total cell density and is given by

$$N(t,\mathbf{x}) = \int_V \int_Y p(t,\mathbf{x},\mathbf{v},y)dy\ d\mathbf{v} + \int_Y r(t,\mathbf{x},y)dy,$$

and $g(N)$ and $l(N)$ are functions representing *gain* and *loss* due to cell death and proliferation. α and β are the rates with which cells stop and proliferate, respectively start moving after a resting (proliferating) phase. Thereby, the cells which exit the proliferative phase and start to move are doing this by interacting with the tissue. [5] Both α and β may depend on the position $\mathbf{x}$.

2.2. **Cell surface receptor dynamics.** As in [16], we focus on the cell surface receptor dynamics. Transmembrane adhesion proteins bind to unsoluble proteins available in the brain tissue. In this work we want to study the impact of this microscopic process on the macroscopic movement behaviour on the tissue scale. Starting from simple mass action kinetics, the receptor binding dynamics on the cell surface is described by the following ordinary differential equation:

$$\dot{y} = k^+(R_0 - y)A - k^- y, \tag{3}$$

where R_0 denotes the total number of receptors on the cell (we assume it is conserved), whereas $y(t)$ gives the density of receptors bound to tissue fibers. The constants k^+ and k^- denote the reaction rates for the reversible binding. The steady state of equation (3) is given by $y^* = \frac{k^+ A R_0}{k^+ A + k^-}$. Following [16, 18] we introduce a new internal variable $z := y^* - y$ measuring deviations from the steady state. Assuming that the receptor binding process is fast and equilibrates rapidly, these deviations will be very small and this will allow us later on to close the moments system in Subsection 2.3.

Next consider the path of a single cell starting in $\mathbf{x}_0$ and moving with velocity $\mathbf{v}$ through a time-invariant density field $A(\mathbf{x})$. Then with the notations $\mathbf{x} = \mathbf{x}_0 + \mathbf{v}t$ and

$$f(A(\mathbf{x})) = \frac{k^+ A(\mathbf{x}) R_0}{k^+ A(\mathbf{x}) + k^-}$$

it follows that for any t

$$\frac{d}{dt} f\big(A(\mathbf{x}_0 + \mathbf{v}t)\big) = f'(A(\mathbf{x}_0 + \mathbf{v}t))\ \mathbf{v} \cdot \nabla A(\mathbf{x}_0 + \mathbf{v}t)$$

and hence z satisfies the equation

$$\begin{aligned} \dot{z} &= -(k^+ A(\mathbf{x}) + k^-)z + f'(A(\mathbf{x}))\mathbf{v} \cdot \nabla A(\mathbf{x}) \\ &= -(k^+ A(\mathbf{x}) + k^-)z + \frac{k^+ k^- R_0}{(k^+ A(\mathbf{x}) + k^-)^2}\ \mathbf{v} \cdot \nabla A(\mathbf{x}). \end{aligned}$$

This equation can be solved explicitly for z to yield

$$z(t) = (y^* - y_0)e^{-(k^+ A + k^-)t} + (1 - e^{-(k^+ A + k^-)t})\frac{k^+ k^- R_0}{(k^+ A + k^-)^3}\ \mathbf{v} \cdot \nabla A,$$

where $y_0 = y(0)$. Hence, z is bounded as long as ∇A is and its sign depends on the current orientation of the cell w.r.t. the gradient of the fiber volume fraction.

[5] The importance of cell-tissue interactions (via receptor bindings to the nonsoluble ligands on the tissue fibers) for cell division has been experimentally put in evidence, see e.g., [33].

We choose the turning rate to be of the form $\lambda(z) = \lambda_0 - \lambda_1 z \geq 0$, where λ_0 and λ_1 are some positive constants. Note that this is equivalent to considering $\lambda(y) = \lambda_0 - \lambda_1 y^* + \lambda_1 y$, which becomes indeed larger when many receptors are bound to fibers.[6] This choice corresponds to the one proposed in [18] for the turning rate of bacteria and – after a linearization – also to that chosen in [23].

2.3. **The mesoscopic transport equation and its scaling.** With the above analysis for the dynamics on the microscale, we obtain now a system of evolution equations for the density $p(t, \mathbf{x}, \mathbf{v}, z)$ of moving cells and the density $r(t, \mathbf{x}, z)$ of resting cells. The system reads

$$\begin{aligned} \partial_t p + \mathbf{v}\cdot\nabla p \,+\, \partial_z\big(\big(-(k^+A + k^-)z + f'(A)\mathbf{v}\cdot\nabla A\big)p\big) = \\ \mathcal{L}[\lambda_0]p - \mathcal{L}[\lambda_1]zp - \alpha(\mathbf{x})p + \frac{q\beta}{\omega}r - l(N)p \end{aligned} \tag{4a}$$

$$\partial_t r = \alpha(\mathbf{x})\int_V p d\mathbf{v} - \beta r + (g(N) - l(N))\, r. \tag{4b}$$

In the following we consider the moments w.r.t. the involved distribution functions[7] and introduce the notations

$$m = \int_Z p dz, \qquad w = \int_Z r dz, \tag{5a}$$

$$m^z = \int_Z z p dz, \qquad w^z = \int_Z z r dz, \tag{5b}$$

$$M = \int_V m d\mathbf{v}, \qquad M^z = \int_V m^z d\mathbf{v}, \tag{5c}$$

where $Z \subseteq [y^* - R_0, y^*]$ is our new domain for the internal dynamics. In the following we assume the functions to have a relatively compact support in this interval and be compactly supported in the $(\mathbf{x}, \mathbf{v})$-space, which allows to perform the subsequent calculations.

Integration of the equations (4a) and (4b) with respect to z gives

$$\partial_t m + \mathbf{v}\cdot\nabla m = \mathcal{L}[\lambda_0]m - \mathcal{L}[\lambda_1]m^z - \alpha m + \frac{\beta q}{\omega}w - l(N)m, \tag{6a}$$

$$\partial_t w = \alpha(\mathbf{x})M - \beta w + (g(N) - l(N))\, w. \tag{6b}$$

Multiply equations (4a) and (4b) by z and integrate again with respect to z. As in [16] we neglect moments of higher order in z (assuming that the internal dynamics equilibrates rapidly, so that the system is close to the steady state) and obtain

$$\begin{aligned} \partial_t m^z + \mathbf{v}\cdot\nabla m^z = &-(k^+A + k^-)m^z + f'(A)\mathbf{v}\cdot\nabla A\; m \\ &+ \mathcal{L}[\lambda_0]m^z - \alpha m^z + \frac{\beta q}{\omega}w^z - l(N)m^z, \end{aligned} \tag{7a}$$

$$\partial_t w^z = \alpha M^z - \beta w^z + g(N)w^z - l(N)w^z. \tag{7b}$$

[6] Notice that the receptor binding happens all over the cell surface, rather than just on one side of it; hence the cell will have many options to choose its movement direction, according to the – possibly fast – changing informations it obtains from these bindings.

[7] this approach was used previously in [18] in a related context

Now, we use a parabolic scaling $\hat{t} \to \varepsilon^2 t$, $\hat{\mathbf{x}} \to \varepsilon \mathbf{x}$, then drop the hats for notational simplification. In addition, we scale the birth-death dynamics as in [26] by

$$g(N) \to \varepsilon^2 \hat{g}(\hat{N})$$
$$l(N) \to \varepsilon^2 \hat{l}(\hat{N}).$$

This relies on the assumption that the time scale on which birth and death events occur is much slower than the random walk process. From equations (6a), (6b), (7a) and (7b) we obtain

$$\begin{aligned}
\varepsilon^2 \partial_t m + \varepsilon \mathbf{v} \cdot \nabla m &= \mathcal{L}[\lambda_0]m - \mathcal{L}[\lambda_1]m^z - \alpha m + \frac{\beta q}{\omega} w - \varepsilon^2 l(N) m, \\
\varepsilon^2 \partial_t w &= \alpha(\mathbf{x}) M - \beta w + \varepsilon^2 \left(g(N) - l(N)\right) w, \\
\varepsilon^2 \partial_t m^z + \varepsilon \mathbf{v} \cdot \nabla m^z &= -(k^+ A + k^-) m^z + \varepsilon f'(A) \mathbf{v} \cdot \nabla A \; m \\
&\quad + \mathcal{L}[\lambda_0]m^z - \alpha m^z + \frac{\beta q}{\omega} w^z - \varepsilon^2 l(N) m^z \\
\varepsilon^2 \partial_t w^z &= \alpha M^z - \beta w^z + \varepsilon^2 \left(g(N) - l(N)\right) w^z.
\end{aligned}$$

Next we use Hilbert expansions for m, m^z, w, w^z, M, M^z of the form

$$\begin{aligned}
m &= m_0 + \varepsilon m_1 + \varepsilon^2 m_2 + \dots, & M &= M_0 + \varepsilon M_1 + \varepsilon^2 M_2 + \dots \\
m^z &= m_0^z + \varepsilon m_1^z + \varepsilon^2 m_2^z + \dots, & M^z &= M_0^z + \varepsilon M_1^z + \varepsilon^2 M_2^z + \dots \\
w &= w_0 + \varepsilon w_1 + \varepsilon^2 w_2 + \dots, & w^z &= w_0^z + \varepsilon w_1^z + \varepsilon^2 w_2^z + \dots
\end{aligned}$$

and compare terms of equal order in ε.

ε^0 :

$$0 = \mathcal{L}[\lambda_0]m_0 - \mathcal{L}[\lambda_1]m_0^z - \alpha m_0 + \frac{\beta q}{\omega} w_0, \tag{8a}$$
$$0 = \alpha M_0 - \beta w_0, \tag{8b}$$
$$0 = -(k^+ A + k^-) m_0^z - \alpha m_0^z + \frac{\beta q}{\omega} w_0^z + \mathcal{L}[\lambda_0]m_0^z, \tag{8c}$$
$$0 = \alpha M_0^z - \beta w_0^z. \tag{8d}$$

ε^1 :

$$\mathbf{v} \cdot \nabla m_0 = \mathcal{L}[\lambda_0]m_1 - \mathcal{L}[\lambda_1]m_1^z - \alpha m_1 + \frac{\beta q}{\omega} w_1, \tag{9a}$$
$$0 = \alpha M_1 - \beta w_1, \tag{9b}$$
$$\mathbf{v} \cdot \nabla m_0^z = -(k^+ A + k^-) m_1^z + f'(A) \mathbf{v} \cdot \nabla A \; m_0 + \mathcal{L}[\lambda_0]m_1^z - \alpha m_1^z + \frac{\beta q}{\omega} w_1^z, \tag{9c}$$
$$0 = \alpha M_1^z - \beta w_1^z. \tag{9d}$$

ε^2 :

$$\partial_t m_0 + \mathbf{v} \cdot \nabla m_1 = \mathcal{L}[\lambda_0]m_2 - \mathcal{L}[\lambda_1]m_2^z - \alpha m_2 + \frac{\beta q}{\omega} w_2 - l(N_0) m_0, \tag{10a}$$
$$\partial_t w_0 = \alpha M_2 - \beta w_2 + \left(g(N_0) - l(N_0)\right) w_0. \tag{10b}$$

It is our goal now to derive an evolution equation for the macroscopic cell density

$$N_0(t, \mathbf{x}) = w_0 + M_0 = \left(1 + \frac{\alpha}{\beta}\right) M_0. \tag{11}$$

We start with the equations for the coefficients of ε^0. First of all, we obtain from (8d) that $w_0^z = \frac{\alpha}{\beta} M_0^z$. Integration of (8c) with respect to $\mathbf{v}$ yields (recall the notations (2), (5b) and (5c)):

$$0 = -(k^+ A + k^-) M_0^z - \alpha M_0^z + \beta w_0^z,$$

which implies $M_0^z = 0$, $m_0^z = 0$ and $w_0^z = 0$. Equation (8b) gives

$$w_0 = \frac{\alpha}{\beta} M_0. \tag{12}$$

Finally, we obtain from (8a) by using (12) and $m_0^z = 0$ deduced above that

$$0 = \mathcal{L}[\lambda_0] m_0 - \alpha m_0 + \frac{q\alpha}{\omega} M_0, \text{ from which } m_0 = \frac{q}{\omega} M_0.$$

Now let us analyze the equations for the coefficients of ε^1. Starting with eq. (9d) we obtain

$$w_1^z = \frac{\alpha}{\beta} M_1^z.$$

From equation (9c) we obtain after integration with respect to $\mathbf{v}$ that $M_1^z = 0$ and hence also $w_1^z = 0$. Here we used the assumption $\int \mathbf{v} q \, d\mathbf{v} = 0$ for undirected tissue. Then, again from (9c) we obtain the following expression for m_1^z:

$$m_1^z = \frac{1}{k^+ A + k^- + \lambda_0 + \alpha} f'(A) \mathbf{v} \cdot \nabla A \; m_0.$$

Equation (9a) leads to the expression

$$\mathbf{v} \cdot \nabla m_0 = \mathcal{L}[\lambda_0 + \alpha] m_1 + \lambda_1 m_1^z.$$

Now use the properties of the operator $\mathcal{L}[\lambda_0 + \alpha]$ defined on the weighted L^2-space $L_q^2(V)$ [27]. Thereby, the weight function is $q^{-1}(\hat{\mathbf{v}})$ and $\mathcal{L}[\lambda_0 + \alpha]$ is a compact Hilbert-Schmidt operator (see [28]) whose kernel is given by the linear space $\langle q \rangle$, denoting the subspace of $L_q^2(V)$ spanned by q. The pseudoinverse $\mathcal{L}[\lambda_0 + \alpha]^{-1}_{|<q>^\perp}$ of this operator (see again [28] or [16]) is just the multiplication by the factor $-\frac{1}{\lambda_0 + \alpha}$.

This leads to

$$m_1 = -\frac{1}{\lambda_0 + \alpha} \left(\mathbf{v} \cdot \nabla m_0 - \lambda_1 m_1^z \right).$$

Using equations (10a) and (10b) we can derive an evolution equation for the macroscopic cell density (11). From (10b) we have

$$\frac{\beta}{\omega} w_2 = \frac{1}{\omega} \left(\alpha M_2 + (g(N_0) - l(N_0)) \, w_0 - \partial_t w_0 \right).$$

Plugging this term into equation (10a) we obtain

$$\begin{aligned} \partial_t m_0 + \mathbf{v} \cdot \nabla m_1 = \mathcal{L}[\lambda_0] m_2 - \mathcal{L}[\lambda_1] m_2^z - \alpha m_2 + \frac{\alpha q}{\omega} M_2 \\ + \frac{q}{\omega} \left(g(N_0) - l(N_0) \right) \frac{\alpha}{\beta} M_0 - \frac{q}{\omega} \partial_t \left(\frac{\alpha}{\beta} M_0 \right) - l(N_0) m_0. \end{aligned}$$

After integrating again with respect to $\mathbf{v}$ this yields

$$\partial_t M_0 + \int_V \mathbf{v} \cdot \nabla m_1 \; d\mathbf{v} = \left(g(N_0) - l(N_0) \right) \frac{\alpha}{\beta} M_0 - \frac{\alpha}{\beta} \partial_t M_0 - l(N_0) M_0.$$

Rearranging gives

$$\partial_t \left(1 + \frac{\alpha}{\beta} \right) M_0 + \nabla \cdot \int_V \mathbf{v} m_1 \; d\mathbf{v} = \frac{\alpha}{\beta} g(N_0) M_0 - \left(1 + \frac{\alpha}{\beta} \right) M_0 l(N_0).$$

With the defined macroscopic quantity

$$N_0 = \left(1 + \frac{\alpha}{\beta}\right) M_0$$

we obtain

$$\partial_t N_0 + \nabla \cdot \int_V \mathbf{v} m_1 \, d\mathbf{v} = \frac{\alpha}{\alpha+\beta} g(N_0) N_0 - N_0 l(N_0).$$

Now evaluate $\int_V \mathbf{v} m_1 d\mathbf{v}$. Recall

$$m_1 = -\frac{1}{\lambda_0 + \alpha} \left(\mathbf{v} \cdot \nabla \left(\frac{q}{\omega} M_0 \right) - \lambda_1 m_1^z \right). \tag{13}$$

Writing $\gamma(\mathbf{x}) = \frac{1}{k^+ A + k^- + \lambda_0 + \alpha}$ and hence $m_1^z = \gamma(\mathbf{x}) f'(A) \mathbf{v} \cdot \nabla A \; m_0$ we have

$$m_1 = -\frac{1}{\lambda_0 + \alpha} \left(\mathbf{v} \cdot \nabla \left(\frac{q}{\omega} M_0 \right) - \lambda_1 \gamma(\mathbf{x}) f'(A) \mathbf{v} \cdot \nabla A \frac{q}{\omega} M_0 \right).$$

It follows

$$\begin{aligned}
\nabla \cdot \int_V \mathbf{v} m_1 \, d\mathbf{v} &= \nabla \cdot \left(-\frac{1}{\lambda_0 + \alpha} \int_V \mathbf{v}\mathbf{v}^t \nabla \left(\frac{q}{\omega} M_0 \right) d\mathbf{v} \right) \\
&\quad + \nabla \cdot \left(\frac{\lambda_1}{\lambda_0 + \alpha} \int_V \mathbf{v}\mathbf{v}^t \frac{q}{\omega} \, d\mathbf{v} \gamma(\mathbf{x}) f'(A) \nabla A M_0 \right) \\
&= \nabla \cdot \left(-\frac{1}{\lambda_0 + \alpha} \nabla \cdot \left(\frac{1}{\omega} \int_V \mathbf{v}\mathbf{v}^t q \, d\mathbf{v} \; M_0 \right) \right) \\
&\quad + \nabla \cdot \left(\frac{\lambda_1}{\lambda_0 + \alpha} \gamma(\mathbf{x}) f'(A) \frac{1}{\omega} \int_V \mathbf{v}\mathbf{v}^t q \, d\mathbf{v} \; \nabla A M_0 \right).
\end{aligned}$$

Finally, we obtain with $M_0 = \frac{\beta}{\alpha+\beta} N_0$ and

$$\mathbb{D}_T(\mathbf{x}) = \frac{1}{\omega} \int_V \mathbf{v}\mathbf{v}^t q \, d\mathbf{v} \tag{14}$$

the evolution equation

$$\begin{aligned}
&\partial_t N_0 - \nabla \cdot \left(\frac{1}{\lambda_0 + \alpha(\mathbf{x})} \nabla \cdot \left(\frac{\beta}{\alpha(\mathbf{x}) + \beta} \mathbb{D}_T(\mathbf{x}) N_0 \right) \right) \\
&\quad + \nabla \cdot \left(\frac{\lambda_1}{\lambda_0 + \alpha(\mathbf{x})} \gamma(\mathbf{x}) f'(A) \frac{\beta}{\alpha(\mathbf{x}) + \beta} \mathbb{D}_T(\mathbf{x}) \cdot \nabla A \; N_0 \right) \\
&\quad = \frac{\alpha(\mathbf{x})}{\alpha(\mathbf{x}) + \beta} g(N_0) N_0 - N_0 l(N_0).
\end{aligned} \tag{15}$$

Notice that we still have to determine the form of q in order to obtain an explicit expression for the tumor diffusion tensor $\mathbb{D}_T(\mathbf{x})$.

2.4. **Determination of the coefficients.** Now we are interested in the form of the diffusion tensor $\mathbb{D}_T(\mathbf{x})$ in equation (14). To determine its specific form we have to choose a concrete form for the fiber distribution q. As shown in [16, 39], a possible choice can be

$$q(\mathbf{x}, \boldsymbol{\theta}) = \frac{n}{|\mathbb{S}^{n-1}| \operatorname{tr} \mathbb{D}_W(\mathbf{x})} \boldsymbol{\theta}^t \mathbb{D}_W(\mathbf{x}) \boldsymbol{\theta}. \tag{16}$$

Thereby, $\mathbb{D}_W(\mathbf{x})$ is the *water diffusion tensor* and can be obtained for each voxel $\mathbf{x}$ by DTI measurements, n denotes the space dimension, and $\mathbb{S}^{n-1}$ is the unit sphere in $\mathbb{R}^n$.

Another choice proposed in [39] is the bimodal von Mises-Fisher distribution

$$q(\mathbf{x},\boldsymbol{\theta}) = \frac{k(\mathbf{x})}{8\pi \sinh(k(\mathbf{x}))}\left(e^{k\boldsymbol{\phi}\cdot\boldsymbol{\theta}} + e^{-k\boldsymbol{\phi}\cdot\boldsymbol{\theta}}\right), \tag{17}$$

with $k(\mathbf{x}) = \kappa \cdot \mathrm{FA}(\mathbf{x})$, where $\mathrm{FA}(\mathbf{x})$ denotes the fractional anisotropy and $\boldsymbol{\phi}$ represents the leading eigenvector of the water diffusion tensor $\mathbb{D}_W(\mathbf{x})$. This latter distribution was found in [39] to be more adequate for the description of the cells following the tissue anisotropy. However, it is not clear how to choose the concentration parameter κ for the sensitivity of the cells to the orientation of the underlying fiber structure. The simulations performed in [16] hinted on both choices not being enough to capture the fractal patterns of glioma spread in the framework of a single scale model.

Each of the above formulae (16) and (17) allows for computing the fiber distribution function for each voxel. In the following we choose to work with (16). In [39] it has first been shown that for this choice the tensor (14) has the form (recall that s denotes the speed of the cells – which we assumed to be constant – and λ_0 is one of the coefficients in the cells' turning rate λ depending on the receptor binding state; $\mathbb{I}_n$ denotes the identity matrix in $\mathbb{R}^{n\times n}$)

$$\mathbb{D}_T(\mathbf{x}) = \frac{s^2}{\lambda_0(n+2)}\left(\mathbb{I}_n + 2\frac{\mathbb{D}_W(\mathbf{x})}{\operatorname{tr}\mathbb{D}_W(\mathbf{x})}\right), \tag{18}$$

which was reconsidered for the tumor diffusion tensor computed in [16]. The rates α and β introduced in Subsection 2.1 are assumed not to vary drastically within the brain, and hence to be constant in space.

2.5. **The full macroscopic model.** For the sake of clarity we collect the results of our calculations and formulate the whole macroscopic model again. We obtained from our scaling an approximating partial differential equation of advection-diffusion-reaction type for the macroscopic cell density N_0. We assume that the transition rates α and β between the two subpopulations or moving/proliferating cells do not vary in space and furthermore – just to make a choice – assume that the proliferation is logistic[8]. Specifying the growth and depletion functions g and l to be of the form $g(N_0) = c_g$ and $l(N_0) = c_l N_0$, respectively, with appropriate positive constants $c_g, c_l \in \mathbb{R}$, we obtain the equation

$$\partial_t N_0 - c_D \nabla\nabla\left(\mathbb{D}_T(\mathbf{x})N_0\right) \underbrace{- \lambda_1 c_D \nabla\left(\mathbf{u}(\mathbf{x})N_0\right)}_{\text{haptotactic term}} = \underbrace{\frac{\alpha}{\alpha+\beta}c_g N_0 - c_l N_0^2}_{\text{proliferation term}}, \tag{19}$$

with $c_D = \frac{\beta}{(\lambda_0+\alpha)(\alpha+\beta)}$ and $\mathbf{u}(\mathbf{x}) = \gamma(\mathbf{x})f'(A(\mathbf{x}))\mathbb{D}_T(\mathbf{x})\nabla A N_0$. Thereby $\mathbb{D}_T$ is the tumor diffusion tensor obtained in (18) and $\gamma(\mathbf{x})$ denotes the function introduced after (13) and depending among other on the macroscopic volume fraction of tissue A. Recall the constants λ_0 and λ_1 are involved in the turning rate of the cells.

3. **Numerical simulations.** We present 2D simulations of the resulting macroscopic advection-diffusion-reaction equation (19). The tumor diffusion tensor, the tumor drift velocity, and the local growth rates are precalculated using MATLAB[9]. The simulations of the macroscopic evolution equation are implemented using the DUNE framework [2, 3].

[8] of course, other choices are possible as well

[9] MATLAB Release 2012b, The MathWorks, Inc., Natick, Massachusetts, United States.

The macroscopic quantities $\mathbb{D}_T(\mathbf{x})$ and $\mathbf{u}(\mathbf{x})$ are spatially dependent, and we expect regions in space where the system is diffusion dominated and regions where it is drift dominated. This can be expressed by the spatially dependent Péclet number $\mathrm{Pe} = \frac{\|\mathbf{u}(\mathbf{x})L\|}{\|\mathbb{D}_T(\mathbf{x})\|}$, where the norm in the numerator is the L^2 norm, while we take in the denominator the Frobenius norm of $\mathbb{D}_T$. L is a macroscopic characteristic length scale (i.e. a mesh width of 2 mm, in our present setting and simulations). For $\mathrm{Pe} \ll 1$ the equation is diffusion dominated, and classical methods for parabolic equations will apply, while for $\mathrm{Pe} \gg 1$ it is drift dominated, and hyperbolic numerical methods must be used. Note that the equation is still parabolic, but the numerical method should be chosen based on its characteristic scales.

The numerical scheme needs to be able to handle nonlinear degenerated anisotropic parabolic equations and full tensors. Furthermore, it should be locally mass conservative. For these reasons we decided to use a first order discontinuous Galerkin (dG) scheme in space and an implicit Euler scheme in time. The nonlinearities are handled using an outer Newton scheme for each time step. This method is overall first order accurate.

3.1. **Spatial discretization.** For the spatial discretization we use a structured mesh $\mathcal{M}(\Omega) = \{E_i\}$, which is a subset of the voxel mesh of the DTI data. Since our mesh is Cartesian with mesh-width h, the sets E_i are simply the grid cells that belong to the brain tissue. We define the skeleton of $\mathcal{M}$ as the boundary between those grid cells, $\Gamma = \{\gamma_{e,f} = \partial E_e \cap \partial E_f \ : \ E_e, E_f \in \mathcal{M},\ E_e \neq E_f,\ \text{and } |\gamma_{e,f}| > 0\}$.

We use a symmetric interior penalty discontinuous Galerkin method (SIPG) [49] as implemented in DUNE [3]. We denote with V_h the dG trial- and test space, which is in our case the space of piecewise bilinear polynomials

$$V_h = \left\{ \nu_h \in L^2(\Omega) \ : \ \nu_h|_E \in Q_1(E), E \in \mathcal{M}(\Omega) \right\},$$

where $Q_1(E)$ denotes the set of bilinear functions on E.

We test the above equation (19) with these ansatz functions, use a weak formulation, and express coupling conditions along the skeleton through jumps $[\![\cdot]\!]$ and averages $\{ \cdot \}$ in a similar notation as in [1]. We use weighted averages, as proposed in [19]. Omitting the computational details, which can be found for example in [1], the resulting semi-discrete problem reads:

Find $N_{0h}(t) \in V_h$ such that

$$\partial_t N_{0h}(t) + a_h\big(N_{0h}(t), \nu_h\big) + J_h\big(N_{0h}(t), \nu_h\big) = R(N_{0h}) \qquad \forall \nu_h \in V_h, \tag{20}$$

with a nonlinear reaction term R, the bilinear form a_h, and a penalty term J_h given by

$$R(N_{0h}(t)) = \frac{\alpha}{\alpha+\beta} c_g N_{0h}(t) - c_l N_{0h}(t)^2, \tag{21}$$

$$\begin{aligned} a_h\big(N_{0h}(t), \nu_h\big) = &\int_\Omega c_D \mathbb{D}_T \nabla N_{0h}(t) \cdot \nabla \nu_h \, dx \\ &- \int_\Gamma [\![N_{0h}(t)]\!] \cdot \{ c_D \mathbb{D}_T \nabla \nu_h \} + [\![\nu_h]\!] \cdot \{ c_D \mathbb{D}_T \nabla N_{0h}(t) \} \, ds \\ &+ \int_\Omega (\lambda_1 c_D \mathbf{u} \, N_{0h}(t)) \cdot \nabla \nu_h \, dx - \int_\Gamma [\![\nu_h]\!] \cdot (\lambda_1 c_D \mathbf{u} \, N_{0h}^{\uparrow}(t)) ds, \end{aligned} \tag{22}$$

and

$$J_h\big(N_{0h}(t),\nu_h\big) = \eta h^{-1} \int_\Gamma [\![\, N_{0h} \,]\!][\![\, \nu_h \,]\!]\, ds\,, \tag{23}$$

where $\eta > 0$ denotes the penalty factor. For a good choice of η we refer to [19].

Note that we require the normal velocity to be continuous, i.e. $\mathbf{u}|_{\partial E_n}\mathbf{n}_n = -\mathbf{u}|_{\partial E_m}\mathbf{n}_m$, where $\mathbf{n}_n$ denotes the outer normal vector of grid cell E_n. To ensure this, we use a Raviart-Thomas RT0 approximation of the velocity field. On an internal edge with two adjacent cells E_n and E_m we define $[\![\, x \,]\!] = x|_{\partial E_n}\mathbf{n}_n + x|_{\partial E_m}\mathbf{n}_m$ and $\{\, x \,\} = \omega_n x|_{\partial E_n} + \omega_m x|_{\partial E_m}$, with weights ω_n, ω_m and the unit outer normal vectors $\mathbf{n}_n, \mathbf{n}_m$. To be robust with respect to heterogeneous diffusion coefficients, we use the weights $\omega_n = \frac{\mathbf{n}_n^t \mathbb{D}_{Tn}\mathbf{n}_n}{\mathbf{n}_n^t(\mathbb{D}_{Tn}+\mathbb{D}_{Tm})\mathbf{n}_n}$ and $\omega_m = \frac{\mathbf{n}_m^t \mathbb{D}_{Tm}\mathbf{n}_m}{\mathbf{n}_m^t(\mathbb{D}_{Tn}+\mathbb{D}_{Tm})\mathbf{n}_m}$ respectively, where $\mathbb{D}_{Tn}$ denotes the tumor diffusion tensor computed in E_n. Note that due to $\mathbf{n}_n = -\mathbf{n}_m$ the relation $\omega_n + \omega_m = 1$ holds.

The advective term is stabilized using an upwind formulation, with the upwind reconstruction $N_{0h}^{\uparrow}$ of the cell density.

3.2. **Temporal discretization.** For the time discretization of N_{0h} we use an implicit Euler scheme and choose the time step τ such that the discrete CFL (Courant-Friedrichs-Lewy) condition of $\frac{\tau\,\lambda_1 c_D \|\mathbf{u}\|_\infty}{h} \leq 1$ is satisfied. Note that although the implicit Euler scheme is unconditionally a-stable we should still avoid too large time steps to keep the discretization error low.

For each time step we obtain a nonlinear system, due to the growth term. The modeling of the latter requires that the tumor cell density is positive. The employed dG scheme is stable but not monotone; i.e. small undershoots are possible and will occur in practice. Therefore, we cannot directly compute $R(N_0)$, but employ a clipping at zero. The non-differentiability of the clipped operator at zero would lead to severe problems in the Newton method. Thus, we regularize the clipping with a parameter ϵ, which yields the clipping operator

$$C_\epsilon(N_0) = \begin{cases} 0 & \text{if } N_0 < 0 \\ {N_0}^2/\epsilon & \text{if } N_0 < 0.5\epsilon \\ N_0 - 0.25\epsilon & \text{else}\,. \end{cases}$$

For a time step $k+1$, $k \in [1, N)$, and a discrete time step width of τ, the fully discrete problem now reads: Find $N_{0h}^{k+1} \in V_h$ such that

$$\frac{1}{\tau} M_h N_{0h}^{k+1} + a_h(N_{0h}^{k+1},\nu_h) + J_h(N_{0h}^{k+1},\nu_h) - R(C_\epsilon(N_{0h}^{k+1})) = \frac{1}{\tau} M_h N_{0h}^{k} \qquad \forall \nu_h \in V_h. \tag{24}$$

After regularization of R we can employ a standard Newton scheme. To solve the linearized system a conjugate gradient method with an ILU precoditioner with zero-fill-in is applied.

Table 1 shows the parameter values used in the simulations, the DTI data is taken from measurements presented in [48].

3.3. **Simulation results.** The choice of appropriate terms for the gain and loss functions g and l is still an issue. We assume here – as in the most existing works on the macroscale and as announced in Subsection 2.5 – that cellular proliferation can be described with a logistic growth, and take $g(N_0) = c_g$ be constant for the

Parameter	Value	Source
R_0	10^4	[4]
s	$10^{-6}\frac{\mathrm{m}}{\mathrm{s}}$	[40]
λ_0	$0.1\frac{1}{\mathrm{s}}$	[40]
λ_1	$0.01\frac{1}{\mathrm{s}}$	estimated, [16]
k^+	$0.1\frac{1}{\mathrm{s}}$	estimated, [16]
k^-	$0.1\frac{1}{\mathrm{s}}$	[32]
α	$0.01\frac{1}{\mathrm{s}}$	estimated
β	$0.2\frac{1}{\mathrm{s}}$	estimated
c_g	$10^{-5}\frac{1}{\mathrm{s}}$	estimated
c_l	$10^{-7}\frac{1}{\mathrm{s}}$	estimated

TABLE 1. Parameters used in the simulations.

proliferation rate $c_g \in \mathbb{R}^+$ and $l(N_0) = c_l N_0$ for $c_l \in \mathbb{R}^+$. Altogether this leads to the reaction term

$$\frac{\alpha}{\alpha+\beta} c_g N_0 - c_l N_0^2 = \left(\frac{\alpha}{\alpha+\beta} c_g - c_l N_0 \right) N_0.$$

Simulations of equation (19) have been perfomed on a horizontal brain slice of size 117×142 with a binary inital tumor with value 0.8 placed in the left hemisphere. We use DTI measurements provided by the group of Carsten Wolters (WWU Münster). The preprocessed data include segmentation data, apparent water diffusion tensors, and a brainmask for each voxel of the brain of a healthy adult.
We compare results for three different setups: (A) we simulate the full model (19); (B) we consider the model without subcellular dynamics, i.e. omitting the haptotactic drift term, and (C) we omit proliferation, as in [16].

Figure 1 shows the temporal evolution in all three test cases (A), (B), and (C). To allow for a more detailed comparison, Figure 2 plots the solution along an x- and a y-slice for all three setups. Comparing (A) with the pure diffusion case (B), the tumor spread along fiber tracks is similarly fast (Figure 2, x-slice), but orthogonally to the fiber tracks the pure diffusion model overestimates the tumor spread (Figure 2, y-slice). Note the discontinuity in the y-slice where we cross the CSF (cerebrospinal fluid), through which the cells do not migrate. This is mainly visible in case (B), where the CSF acts as a barrier and leads to mildly anisotropic spread. As in [16], significant anisotropic behavior caused by diffusion alone cannot be observed; this also applies to the case including proliferation. Comparing the full model (A) with the case without proliferation (C), we observe that the absolute values in case (C) are significantly smaller, as we only consider spread without growth. We further notice that proliferation causes sharper gradients (see Figure 2) and the corresponding tumor invasion patterns evolve faster than without proliferation. Still many features of the solution are shared by the cases (A) and (C), such as the location of local maxima or minima.

Considering the haptotactic drift leads to branched structures, as Figure 1 (A) shows. The tumor spreads predominantly in brain white matter; according to the (local) anisotropy, these finger-like patterns have actually been observed in clinical imaging (see e.g., [12, 20]), hence our model (19) is able to predict this behavior, unlike diffusion based models exhibiting a rather isotropic spread.

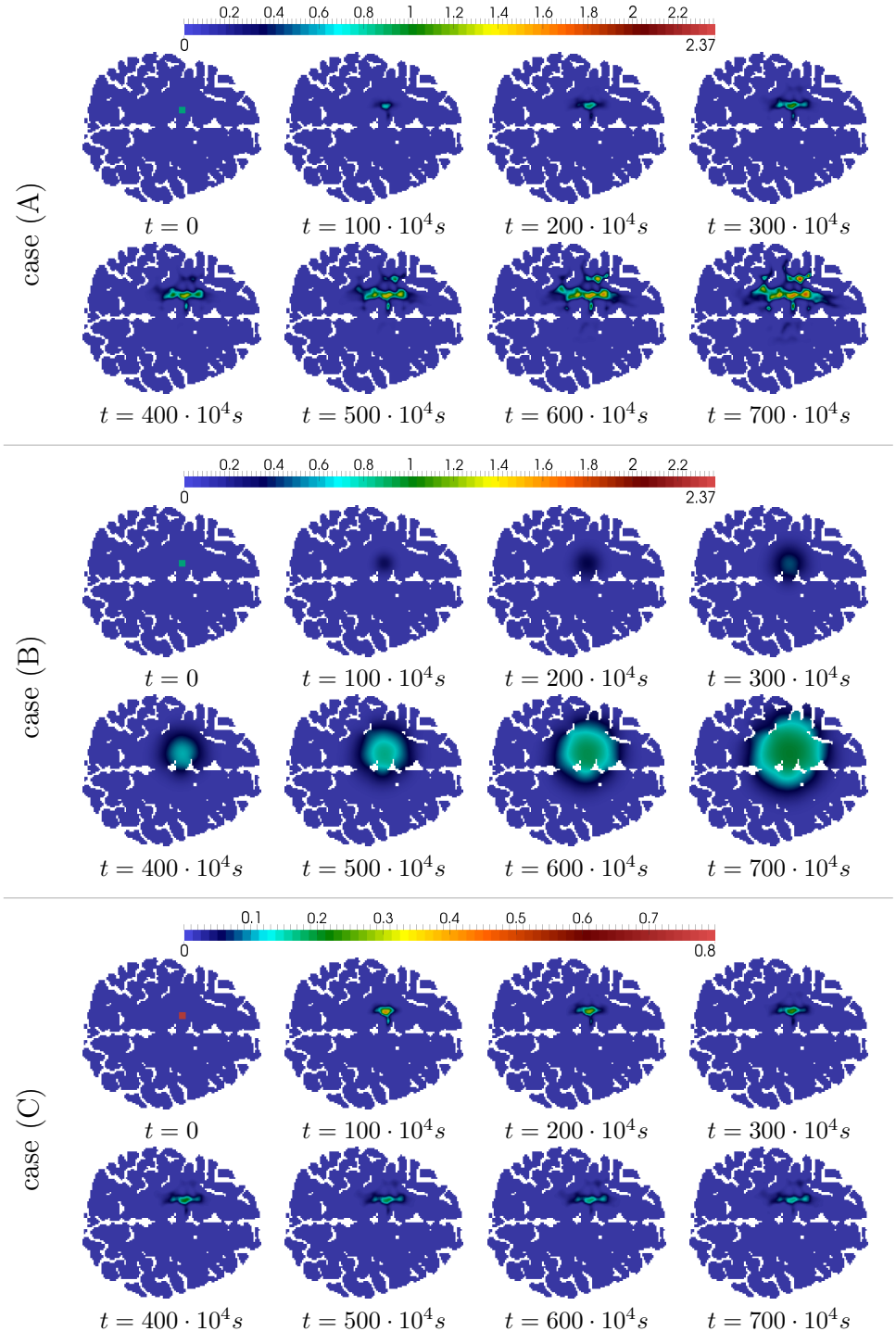

FIGURE 1. Simulation of the evolution equation. Case (A): full model involving subcellular dynamics. Case (B): model without subcellular dynamics (i.e. considering only diffusive transport). Case (C): model without proliferation (as in [16]).

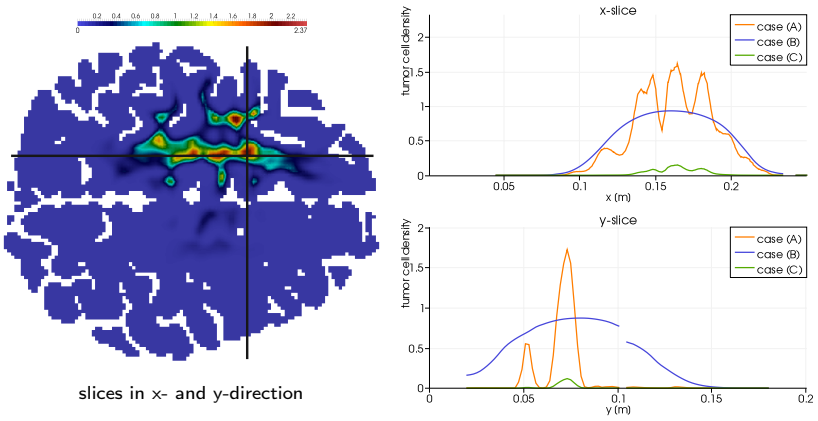

FIGURE 2. Comparison of the full model (left, case (A)) with simulations without subcellular dynamics (case (B)) and without proliferation (case (C)), respectively. Plots of N_0 along an x- and a y-slice. Along the fibers the tumor extent is comparable in case (A) and (B), but orthogonally to the fiber tracks case (B) predicts a much wider spread. Cases (A) and (C) show results with a simular shape: due to missing proliferation, the values in (C) are significantly smaller and the fronts are less sharp. Note the discontinuity in the y-slice where we cross the CSF. As the cells do not travel through the CSF, it acts as a barrier.

4. **Discussion.** The DTI-based multiscale model for glioma invasion proposed and analyzed in this work is an extension of the model introduced in [16]. The novelty is here that we account for proliferation of tumor cells. Thereby, we made use of the go-or-grow dichotomy and identified the resting cells with those proliferating. The choice of gain and loss functions $g(N)$ and $l(N)$ due to cell proliferation and death, as well as of the stopping (growth) rates can be done in a less restrictive way, leading – after the scaling – on the macroscale to rather general proliferation terms, of which the logistic growth (which is commonly chosen when writing some partial differential equations for tumor invasion directly on the population level) is merely a particular case.

The numerical simulations of the macroscopic equation show a highly anisotropic spread of the tumor cells, according to the underlying brain structure. As before in [16] this was achieved by the multiscality of our model (in particular the inclusion of subcellular receptor binding processes and their involvement in the cell turning rates), which led to the dominant haptotactic term in equation (19). When simulating only the pure diffusion model the corresponding invasive behavior is not as often observed clinically, where branched, fingering patterns like those in Figure 1 (A) are the dominating image due to the infiltrative spread of glioma. When compared with our previous multiscale model without proliferation in [16] the present setting predicts – as expected – a faster invasion, with larger cell densities.

The nontrivial issue of modeling cell proliferation in a way which is less artificial than just choosing it to be a logistic growth on the macrolevel was handled here by accounting for the resting (and hence dividing) cells. This, however, is not the only way to characterize it. For instance, Bellomo et al. [5, 6, 7] proposed

to model proliferation on the mesolevel by letting the cells with different internal states[10] interact with each other, which – although intuitive – is (partly) arguable, as cancer cells can divide without needing to stay in (binary) touch with their neighbours. The modeling of cell proliferation on the mesolevel and the deduction of the appropriate mesoscopic equation have been done in [17] after submitting the present paper.

Also observe that through the scaling performed in Subsection 2.3 we obtain an equation for the total tumor cell density, as the latter is the quantity of interest for diagnosis and therapy (e.g., with respect to assessing the degree of the tumor's extent). The tumor heterogeneity relatively to moving (less sensitive) and proliferating (more responsive to treatment) cells is no longer accounted for, as we are primarily concerned with the overall tumor burden. However, the coefficients of our macroscopic equation still carry some of the information contained in the go-or-grow behavior; this information could not have been "guessed" when directly writing a macroscopic equation while merely relying on flux balance.

Acknowledgments. We thank Carsten Wolters and Felix Lucka (Institute of Biomagnetism and Biosignalanalysis, University of Münster) for the preprocessed DTI data. The measurements were first done for [48].

REFERENCES

[1] D. N. Arnold, F. Brezzi, B. Cockburn and L. D. Marini, Unified analysis of discontinuous galerkin methods for elliptic problems, *SIAM Journal on Numerical Analysis*, **39** (2002), 1749–1779.

[2] P. Bastian, M. Blatt, A. Dedner, C. Engwer, R. Klöfkorn, M. Ohlberger and O. Sander, A generic grid interface for parallel and adaptive scientific computing. part I: Abstract framework, *Computing*, **82** (2008), 103–119.

[3] P. Bastian, M. Blatt, A. Dedner, C. Engwer, R. Klöfkorn, R. Kornhuber, M. Ohlberger and O. Sander, A generic grid interface for parallel and adaptive scientific computing. part II: Implementation and tests in DUNE, *Computing*, **82** (2008), 121–138.

[4] A. M. Belkin, G. Tsurupa, E. Zemskov, Y. Veklich, J. W. Weisel and L. Medved, Transglutaminase-mediated oligomerization of the fibrin(ogen) αC domains promotes integrin-dependent cell adhesion and signaling, *Blood*, **105** (2005), 3561–3568.

[5] N. Bellomo, A. Bellouquid, J. Nieto and J. Soler, Complexity and mathematical tools toward the modeling of multicellular growing systems, *Mathematical and Computer Modelling*, **51** (2010), 441–451.

[6] N. Bellomo, A. Bellouquid, J. Nieto and J. Soler, On the asymptotic theory from microscopic to macroscopic tissue models: An overview with perspectives, *Math. Models Methods Appl. Sci.*, **22** (2012), 1130001, 37 pp.

[7] N. Bellomo, D. Knopoff and J. Soler, On the difficult interplay between life, "complexity", and mathematical sciences, *Math. Models Methods Appl. Sci.*, **23** (2013), 1861–1913.

[8] T. Beppu, T.Inoue, Y. Shibata, A. Kurose, H. Arai, K. Ogasawara, A. Ogawa, S. Nakamura and H. Kabasawa, Measurement of fractional anisotropy using diffuson tensor MRI in supratentorial astrocytic tumors, *Journal of Neuro-Oncology*, **63** (2003), 109–116.

[9] K. Böttger, H. Hatzikirou, A. Chauviere and A. Deutsch, Investigation of the migration/proliferation dichotomy and its impact on avascular glioma invasion, *Mathematical Modelling of Natural Phenomena*, **7** (2012), 105–135.

[10] S. Coons, Anatomy and growth patterns of diffuse gliomas, in *The gliomas* (eds. M. Berger and C. Wilson), W.B. Saunders Company, Philadelphia, (1999), 210–225.

[11] G. D'Abaco and A. Kaye, Integrins: Molecular determinants of glioma invasion, *J. of Clinical Neurosci.*, **14** (2007), 1041–1048.

[10] in those papers these are called *activity variables*

[12] C. Daumas-Duport, P. Varlet, M. L. Tucker, F. Beuvon, P. Cervera and J. P. Chodkiewicz, Oligodendrogliomas. Part I: Patterns of growth, histological diagnosis, clinical and imaging correlations: A study of 153 cases, *Journal of Neuro-Oncology*, **34** (1997), 37–59.
[13] T. Demuth and M. E. Berens, Molecular mechanisms of glioma cell invasion and migration, *Journal of Neuro-Oncology*, **70** (2004), 217–228.
[14] M. Descoteaux, R. Deriche, T. R. Knische and A. Anwander, Deterministic and Probabilistic Tractography Based on Complex Fibre Orientation Distributions, *IEEE Transactions on Medical Imaging*, **28** (2009), 269–286.
[15] M. Descoteaux, *High Angular Resolution Diffusion MRI: From Local Estimation to Segmentation and Tractography*, Ph.D. thesis, Université Nice-Sophia Antipolis, 2008.
[16] C. Engwer, T. Hillen, M. Knappitsch and C. Surulescu, Glioma follow white matter tracts: A multiscale DTI-based model, *Journal of Math. Biol.*, **71** (2015), 551–582.
[17] C. Engwer, A. Hunt and C. Surulescu, Effective equations for anisotropic glioma spread with proliferation: A multiscale approach and comparisons with previous settings, *IMA J. Math. Medicine and Biol.*, **32** (2015), doi:10.1093/imammb/dqv030, 2015.
[18] R. Erban and H. Othmer, From signal transduction to spatial pattern formation in *E. coli*: A paradigm for multiscale modeling in biology, *Multiscale Modeling and Simulation*, **3** (2005), 362–394.
[19] A. Ern, A. F. Stephansen and P. Zunino, A discontinuous Galerkin method with weighted averages for advection-diffusion equations with locally small and anisotropic diffusivity, *IMA Journal of Numerical Analysis*, **29** (2009), 235–256.
[20] E. R. Gerstner, P.-J. Chen, P. Y. Wen, R. K. Jain, T. T. Batchelor and G. Sorensen, Infiltrative patterns of glioblastoma spread detected via diffusion MRI after treatment with cediranib, *Neuro-Oncology*, **12** (2010), 466–472.
[21] A. Giese, M. A. Loo, N. Tran, D. Haskett, S. Coons and M. Berens, Dichotomy of astrocytoma migration and proliferation, *International Journal of Cancer*, **67** (1996), 275–282.
[22] A. Giese and M. Westphal, Glioma invasion in the central nervous system, *Neurosurgery*, **39** (1996), 235–252.
[23] D. Grünbaum, Advection-diffusion equations for internal state-mediated random walks, *SIAM Journal for Applied Mathematics*, **61** (2000), 43–73.
[24] D. Hanahan and R. A. Weinberg, Hallmarks of cancer: The next generation, *Cell*, **144** (2011), 646–674.
[25] H. Hatzikirou, D. Basanta, M. Simon, K. Schaller and A. Deutsch, 'Go or Grow': the key to the emergence of invasion in tumour progression?, *Math Med Biol*, **29** (2012), 49–65.
[26] T. Hillen, Transport equations with resting phases, *Europ. J. Appl. Math.*, **14** (2003), 613–636.
[27] T. Hillen, M^5 Mesoscopic and macroscopic models for mesenchymal motion, *Journal of Mathematical Biology*, **53** (2006), 585–616.
[28] T. Hillen and H. Othmer, The diffusion limit of transport equations derived from velocity jump processes, *SIAM Journal on Applied Mathematics*, **61** (2000), 751–775.
[29] K. S. Hoek, O. M. Eichhoff, N. C. Schlegel, U. Döbbeling, S. Hemmi and R. Dummer, In vivo switching of human melanoma cells between proliferative and invasive states, *Cancer Res.*, **68** (2008), 650–656.
[30] J. Kelkel and C. Surulescu, On some models for cancer cell migration through tissue networks, *Mathematical Biosciences and Engineering*, **8** (2011), 575–589.
[31] J. Kelkel and C. Surulescu, A multiscale approach to cell migration in tissue networks, *Mathematical Models and Methods in Applied Sciences*, **23** (2012), 1150017, 25 pp.
[32] D. A. Lauffenburger and J. L. Lindermann, *Receptors. Models for Binding, Trafficking and Signaling*, Oxford University Press, 1993.
[33] K.R. Legate, S.A. Wickström, and R. Fässler, Genetic and cell biological analysis of integrin outside-in signaling, *Genes Dev.*, **23** (2009), 397–418.
[34] T. Lorenz and C. Surulescu, On a class of multiscale cancer cell migration models: Well-posedness in less regular function spaces, *Mathematical Models and Methods in Applied Sciences*, **24** (2014), 2383–2436.
[35] Y. Matsukado, C. MacCarty, J. Kernohan, et al., The growth of glioblastoma multiforme (astrocytomas, grades 3 and 4) in neurosurgical practice, *Journal of Neurosurgery*, **18** (1961), 636–644.
[36] G. Meral, C. Stinner and C. Surulescu, On a multiscale model involving cell contractivity and its effects on tumor invasion, *Discr. Cont. Dyn. Syst. B*, **20** (2015), 189–213.

[37] G. Meral and C. Surulescu, Mathematical Modelling, Analysis and numerical simulations for the influence of the heat shock proteins on tumour invasion, *Journal of Math. Anal. Appl.*, **408** (2013), 597–614.
[38] N. Oppenheimer-Marks and P. E. Lipsky, Adhesion molecules and the regulation of the migration of lymphocytes, in *Adhesion Molecules and Chemokynes in Lymphocyte Trafficking* (ed. A. Hamann), Harwood Acad. Publ. (1997), 55–88.
[39] K.J. Painter and T. Hillen, Mathematical modelling of glioma growth: The use of Diffusion Tensor Imaging (DTI) data to predict the anisotropic pathways of cancer invasion, *J. Theoretical Biol.*, **323** (2013), 25–39.
[40] M. Sidani, D. Wessels, G. Mouneimne, M. Ghosh, S. Goswami, C. Sarmiento, W. Wang, S. Kuhl, M. El-Sibai, J. M. Backer and R. Eddy, D. Soll and J. Condeelis, Cofilin determines the migration behavior and turning frequency of metastatic cancer cells, *The Journal of Cell Biology*, **179** (2007), 777–791.
[41] C. Stinner, C. Surulescu and G. Meral, A multiscale model for pH-tactic tumor invasion with time-varying carrying capacities, *IMA Journal of Applied Mathematics*, **80** (2015), 1300–1321.
[42] C. Stinner, C. Surulescu and M. Winkler, Global weak solutions in a PDE-ODE system modeling multiscale cancer cell invasion, *SIAM J. Math. Analysis*, **46** (2014), 1969–2007.
[43] P. C. Sundgren, Q. Dong, D. Gomez-Hassan, S. K. Mukherji, P. Maly and R. Welsh, Diffusion tensor imaging of the brain: Review of clinical applications, *Neurocarciology*, **46** (2004), 339–350.
[44] Z. Szymanska, J. Urbanski and A. Marciniak-Czochra, Mathematical modelling of the influence of heat shock proteins on cancer invasion of tissue, *Journal of Mathematical Biology*, **58** (2009), 819–844.
[45] D. S. Tuch, Q-ball imaging, *Magnetic resonance in Medicine*, **52** (2004), 1358–1372.
[46] D. S. Tuch, T. G. Reese, M. R. Wiegell and V. J. Wedeen, Diffusion MRI of complex neural architecture, *Neuron*, **40** (2003), 885–895.
[47] J. H. Uhm, C. L. Gladson and J. S. Rao, The role of integrins in the malignant phenotype of gliomas, *Frontiers in Bioscience*, **4** (1999), 188–199.
[48] S. Wagner, S. M. Rampersad, Ü Aydin, J. Vorwerk, T. F. Oostendorp, T. Neuling, C. S. Herrmann, D. F. Stegeman and C. H. Wolters, Investigation of tDCS volume conduction effects in a highly realistic head model, *Journal of neural engineering*, **11** (2014), 016002, 14pp.
[49] M. F. Wheeler, An elliptic collocation-finite element method with interior penalties, *SIAM Journal on Numerical Analysis*, **15** (1978), 152–161.
[50] M. Wrensch, Y. Minn, T. Chew, M. Bondy and M. S. Berger, Epidemiology of primary brain tumors: Current concepts and review of the literature, *Neuro-Oncology*, **4** (2002), 278–299.

Received July 01, 2015; Accepted November 18, 2015.

E-mail address: christian.engwer@uni-muenster.de
E-mail address: markus.knappitsch@uni-muenster.de
E-mail address: surulescu@mathematik.uni-kl.de